

# Unusual water-assisted NO adsorption over Pd/FER calcined at high temperatures: The effect of cation migration

Inhak Song,<sup>a</sup> Konstantin Khivantsev,<sup>a\*</sup> Yiqing Wu,<sup>a</sup> Mark Bowden,<sup>a</sup> Yong Wang,<sup>a,b</sup> and János Szanyi<sup>a\*</sup>

<sup>a</sup>Institute for Integrated Catalysis, Pacific Northwest National Laboratory, Richland, Washington 99352, United States

<sup>b</sup>Voiland School of Chemical Engineering and Bioengineering, Washington State University, Pullman, Washington 99164, United States

\*Corresponding authors: konstantin.khivantsev@pnnl.gov and janos.szanyi@pnnl.gov

**ABSTRACT:** Moisture contained in vehicle exhaust gas normally degrades the capacity and efficiency of Pd ion-exchanged zeolites as NO<sub>x</sub> adsorbents by competitive adsorption on active sites. Here, we report a counterexample to this general proposition, in which moisture facilitates the storage of NO as a nitrosyl complex on hydrated Pd ions in high temperature calcined FER-type zeolites. The divalent Pd<sup>2+</sup> cations upon elevated temperature (>800 °C) calcination occupy sterically constrained cationic positions that render them inactive for the adsorption of probe molecules such as NO. These ‘hidden’ Pd ions, however, are accessible by NO when the zeolite is hydrated, but readily release NO at around 200°C as dehydration proceeds. By combining systematic *in situ* infra-red data with X-ray diffraction Rietveld analyses, we revealed that the high temperature-induced relocation of Pd ions to more stable cationic positions located near 6-membered ring of the ferrierite cage is responsible for this anomalous behavior. This finding constitutes a notable advance in understanding coordination chemistry of cations in zeolites.

## Introduction

Zeolites are crystalline microporous aluminosilicate materials commonly used and intensively studied as adsorbents and catalysts.<sup>1-5</sup> They crystallize in various three-dimensional structures by linking the corner oxygen atoms of silicon or aluminum tetrahedra, i.e., SiO<sub>4</sub> or AlO<sub>4</sub>, in covalent bonds.<sup>6</sup> The formed cavities surrounded by negatively charged framework are charge balanced by metal cations and, normally, surrounded by water molecules.<sup>7-9</sup> Such pores are interconnected to yield channels of molecular dimensions, which allow exchange of cations and transport of reactants.

Although zeolites are now widely utilized, for example, for emission control in vehicles and fluid cracking or hydrocracking in petrochemical industry, there is a lot of chemistry left to discover and to clarify.<sup>10-14</sup> Their unique structures confine molecules into small spaces and alter the reaction pathway by modulating transition states as seen in several examples.<sup>15-17</sup> Zeolites, in general, strongly interact with water, due to the hydrophilic nature of these materials.<sup>18</sup> Clustered water molecules are always present adjacent to Brønsted acid sites under ambient conditions and solvate charge balancing cations and reacting

molecules.<sup>19-20</sup> These confined water molecules have different characteristics from bulk water depending on the shape of the cage and the Al distribution in the framework. A variety of Al ions and ion pairs in zeolite structures provide negative charges to the framework that are charge balanced by mono- or divalent cations. High temperature treatment that can cause dehydration and/or deformation of the framework are known to induce migration of cations to new locations.<sup>21-23</sup>

In emission control technologies the presence of water always needs to be considered.<sup>24-25</sup> Copper ions bound to cationic sites become mobile when they are solvated by water ligands and migrate from cage to cage, making the formation of copper dimers, necessary for re-oxidation in the selective catalytic reduction (SCR), facile.<sup>26-30</sup> In contrast, water is an obstacle in palladium ion exchanged zeolites used as passive NO<sub>x</sub> adsorbers (PNA) at low temperatures.<sup>31-37</sup> In zeolite-based PNAs (SSZ-13, ZSM-5, BEA) Pd ions efficiently trap NO in nitrosyl complexes, i.e., Pd<sup>2+</sup>-NO.<sup>38-46</sup> However, water is always present in the exhaust gas mixture making Pd ions hydrated, i.e., Pd<sup>2+</sup>(H<sub>2</sub>O)<sub>n</sub>, which prevents the coordination of NO molecules. Recently we have reported on the excellent PNA performance of Pd/FER materials.<sup>47</sup> These materials exhibited excellent high temperature hydrothermal stability and cyclability. Interestingly, the best performance of the 1.8 wt% Pd/FER sample was observed after a high temperature (800 °C) calcination step prior to NO<sub>x</sub> exposure. *In situ* FTIR measurements have shown that after calcination at 550 °C most of the Pd ions were present as Pd<sup>2+</sup>(OH<sup>-</sup>) compensating one AlO<sub>2</sub><sup>-</sup> units in the zeolite framework. In contrast, after the high temperature calcination procedure most of the Pd was present as Pd<sup>2+</sup> compensating two AlO<sub>2</sub><sup>-</sup> units. These results suggested that during high temperature calcination Pd ions relocated in the zeolite framework.

In the current study, surprisingly, we observed a counterexample to the known negative effect of water on NO<sub>x</sub> adsorption over Pd ions in ferrierite-type (FER) zeolites. When Pd/FER is annealed under air at high temperatures (800-1000°C), water does not hinder but greatly facilitates NO adsorption. We simultaneously monitored the NO adsorption/desorption behavior and the interaction between adsorbates and Pd cations in real-time by the aid of *in situ* diffuse reflectance Fourier transform infrared spectroscopy coupled with an on-line mass spectrometer (DRIFTS-MS). Here we report on the formation of “hidden” Pd ions (i.e., unable to coordinate NO) at calcination temperature higher than 700 °C, that becomes accessible to NO in the presence of water. These results are rationalized based on the migration of Pd ions between different cationic positions at high temperatures.

## Results and discussion

### Unusual promotion of NO adsorption by water over Pd/FER calcined at 900 °C

A 1.8 wt% Pd/FER with commercial ferrierite zeolite (Si:Al~10) was prepared by a modified ion exchange method as described in our previous studies.<sup>40-41, 47</sup> After calcination at 900°C in air for 5 h (designated as 1.8Pd/FER-900C), we tested the NO adsorption ability of the sample in a DRIFTS-MS system under various conditions (Figure 1a). After loading the sample into the sample holder it was calcined at 500 °C in oxygen and then exposed to the adsorption gas mixture at 100 °C for 30 min. Subsequently, the cell was purged by cutting off NO or NO/CO flows and the sample was heated to 500 °C to observe desorbing species. From a NO+O<sub>2</sub> gas stream (in the absence of H<sub>2</sub>O) only a negligible amount of NO was stored and subsequently released. In contrast, under a wet gas mixture containing NO, O<sub>2</sub>, and H<sub>2</sub>O, much more NO adsorption/desorption was observed compared to dry conditions. This is a very interesting observation since

all reported Pd/zeolite materials performed best under dry condition, i.e., without water during NO<sub>x</sub> adsorption.<sup>31-32</sup> It is known that Pd<sup>2+</sup> ions readily coordinate H<sub>2</sub>O molecules making NO adsorption difficult on hydrated Pd<sup>2+</sup> ions.<sup>32, 43</sup> In contrast, water seems to facilitate NO adsorption over the high temperature calcined Pd/FER-900C material. The addition of 250 ppm CO to wet NO+O<sub>2</sub> stream further enhanced the NO adsorption/desorption amount of this material. Such promoting effect of CO can be explained by the activation of hydrated Pd ions into Pd<sup>2+</sup>(CO)(NO) complex as demonstrated over Pd/SSZ-13 system.<sup>48</sup>

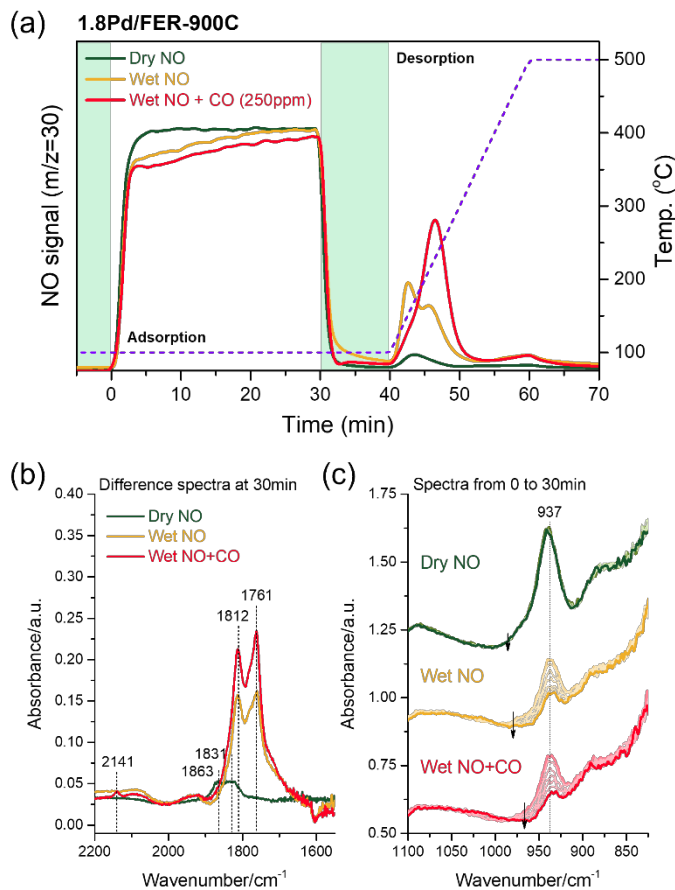


**Figure 1.** (a) NO adsorption and desorption curves for 1.8 wt.% Pd/FER-900C measured by DRIFTS-MS instrument under various conditions. Adsorption gas contained 200 ppm NO, 3% O<sub>2</sub>, 2.8% H<sub>2</sub>O (when used), and 250 ppm CO (when used) balance with He. Desorption of adsorbed NO<sub>x</sub> was performed under 3% O<sub>2</sub>/He (dry) or 3% O<sub>2</sub>+2.8% H<sub>2</sub>O/He (wet) gas with the ramping rate of 20 °C/min. (b) DRIFTS spectra obtained by subtracting two spectra before and after 30 min adsorption of NO under various conditions. (c) Series of spectra (per 5 min) in lower wavenumber region during NO adsorption.

The DRIFTS spectra collected under the three different gas streams after 30 min exposure shows how NO is stored on Pd/FER (Figure 1b). The IR spectra displayed in Figure 1b clearly show that the adsorption complexes formed in the absence and presence of H<sub>2</sub>O are different (i.e., different peak positions). Furthermore, they also reveal, in accordance with the MS data of Figure 1a, that the amount of NO adsorbed are very different (i.e., very small amount of NO in the absence of H<sub>2</sub>O, large amount of NO in the presence of H<sub>2</sub>O and even higher amount of NO when both CO and H<sub>2</sub>O were present). The two IR bands observed at 1863 and 1831 cm<sup>-1</sup> under dry stream are proposed to represent the N-O stretching vibrations of two differently adsorbed NO molecules binding to Pd<sup>2+</sup>(OH) species located in the  $\alpha$ -site in

the large cage and  $\beta$ -site in the 6-membered ring of FER structure, respectively. In the presence of water both of these bands redshift as two high intensity bands develop at 1812 and 1761  $\text{cm}^{-1}$ . The IR feature centered at 1812  $\text{cm}^{-1}$  represents a typical N-O vibration of hydrated  $\text{Pd}^{2+}$ -NO [ $\text{Pd}^{2+}(\text{NO})(\text{H}_2\text{O})_x$ ] that is also observed in other Pd/zeolites.<sup>45, 48</sup> The assignment of the band at 1761  $\text{cm}^{-1}$  is ambiguous. The location of this band is slightly higher than NO adsorbed on metallic Pd which is observed around 1730  $\text{cm}^{-1}$ .<sup>49-50</sup> Under the oxidizing conditions (i.e.,  $\text{NO} + \text{O}_2 + \text{H}_2\text{O}$ ) of these experiments we would not expect to form metallic Pd species anyway. This band, together with that discussed above (i.e., at 1812  $\text{cm}^{-1}$ ), has been assigned to NO molecules coordinated to hydrated  $\text{Pd}^{n+}$  ions.<sup>51</sup> Prior studies also claim that the frequency of N-O stretching vibration can redshift significantly due to hydration of the cationic adsorption center, here  $\text{Pd}^{2+}$ . Therefore, we assign the 1761  $\text{cm}^{-1}$  band to NO molecules adsorbed on hydrated  $\text{Pd}^{2+}$  ions associated with the  $\beta$ -sites. The addition of CO in low concentration (250 ppm) to the gas mixture results in a simultaneous increase in the intensities of the 1812 and 1761  $\text{cm}^{-1}$  IR features and the appearance of a small peak at 2141  $\text{cm}^{-1}$  characteristic of adsorbed CO. In line with our prior study on Pd/CHA, the role of CO is to facilitate Pd-NO formation without influencing the types or distribution of Pd-NO species.<sup>48</sup> These IR measurements, besides providing information about the adsorption complexes formed with CO and NO, can also be used to monitor the interactions of the metal cations in ion exchange positions and the zeolite framework. Zeolite frameworks have their own skeletal vibrations, and the asymmetric T-O-T (T: Si and/or Al) vibrational features can be perturbed by the presence of cations in 2+ oxidation state resulting in the appearance of a vibrational feature that is sensitive to both the nature of the cation and to the adsorbates bound to these cations.<sup>52-56</sup> In our multi-spectroscopy study on Cu/CHA  $\text{NH}_3$ -SCR catalysts we have systematically followed the changes in the asymmetric T-O-T framework vibrational features with variation of the oxidation state of the charge compensating cations as well as the adsorbates bound to these cations.<sup>52</sup> For the Pd/FER sample calcined at 900  $^\circ\text{C}$  we observe a sharp band at 937  $\text{cm}^{-1}$  that represents the perturbed asymmetric T-O-T vibration arising from the interaction between  $\text{Pd}^{2+}$  ions and the FER framework (Figure 1c).<sup>48</sup> This band is absent in the IR spectrum of H/FER (Figure S1). In general, the adsorbate-metal ion (here  $\text{Pd}^{2+}$ ) interaction can lower the intensity and/or shift the peak position of the perturbed T-O-T vibrational feature due to the weakening of the framework-metal ion interaction (moving the Pd ions away from the cationic sites). The asymmetric T-O-T vibrational feature of 1.8 wt% Pd/FER-900C sample at 937  $\text{cm}^{-1}$  remains unchanged during exposure to NO in a dry gas stream, indicating, in agreement with the IR data of Figure 1a, that NO molecules are unable to bind to Pd ions. This result is surprising, in light of evidence that  $\text{Pd}^{2+}$  ions are clearly present in the sample and the zeolite framework is intact after calcination at 900  $^\circ\text{C}$ . However, when water is present in the NO-containing gas stream the intensity of this peak is gradually reduced concomitant with the development of the large NO adsorption features at 1812 and 1761  $\text{cm}^{-1}$ . These changes further accentuated when low concentration (250 ppm) of CO is also included in the simulated exhaust gas stream.

### **The evolution of adsorption sites probed by $\text{H}_2$ TPR, XRD, and CO-DRIFTS**

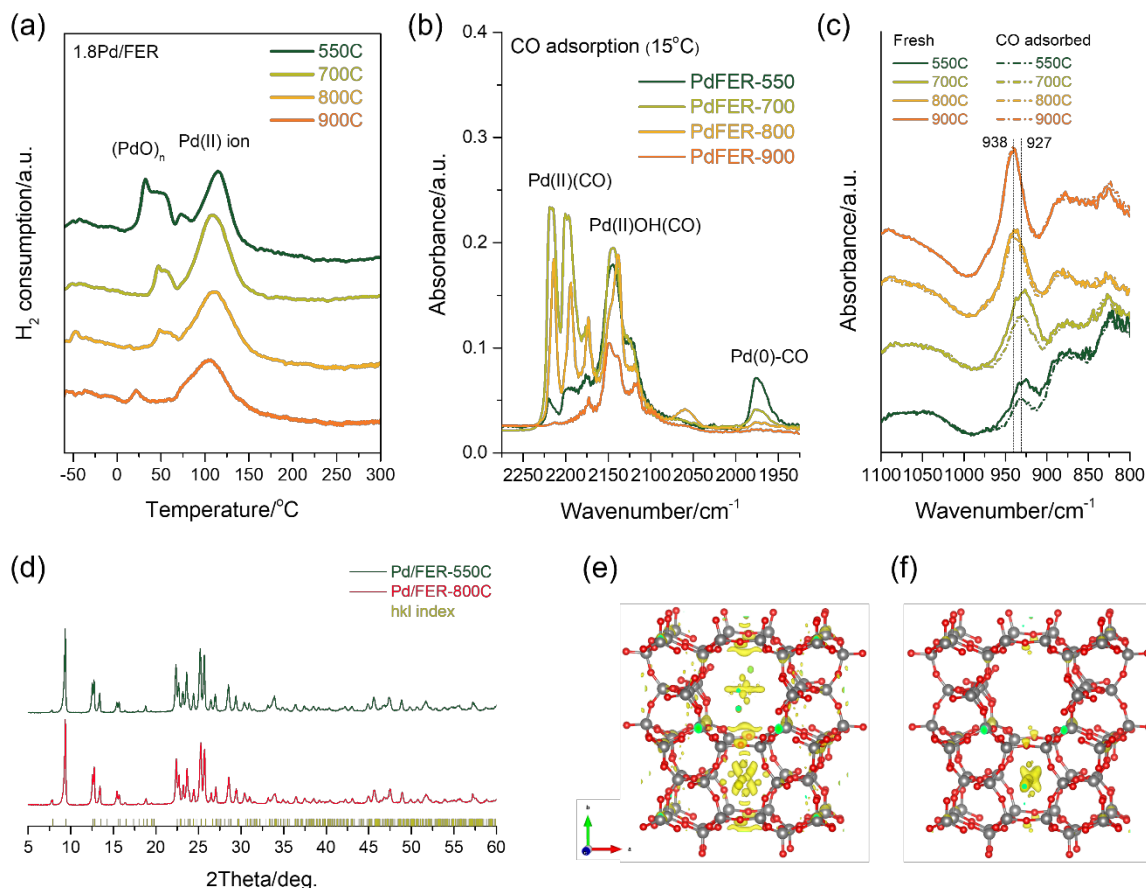


**Figure 2.** (a) Cryo-H<sub>2</sub> temperature programmed reduction profiles for hydrated 1.8Pd/FER samples with different calcination temperatures. Sample was cooled down to -70 °C without pretreatment. (b-c) DRIFTS spectra obtained during CO adsorption at 15 °C for Pd/fer calcined at various temperatures from 550 to 900 °C. Before experiment, the samples were dehydrated at 500 °C for 30 min under 3% O<sub>2</sub>/He. For Pd-CO band, spectrum obtained before flowing CO was subtracted for clearance, while for T-O-T band, the spectra obtained before and after CO adsorption were compared. (d) X-ray diffraction patterns of Pd/fer obtained at 25 °C after in situ thermal oxidative treatments at 550 and 800 °C. Difference electron density map plotted from Rietveld refinement for Pd/fer pre-treated at (e) 550 and (f) 800 °C.

Our prior work on the 1.8 wt% Pd/fer material has revealed that Pd was present both as charge compensation cations [i.e., Pd(OH)<sup>+</sup>] and nano-sized PdO clusters in the zeolite channels (evidenced by TEM analysis) after air calcination at 500 °C.<sup>47</sup> After calcination at 800 °C, however, most of the PdO phase is dispersed in the framework providing charge compensating Pd ions. Using cryogenic H<sub>2</sub> TPR and Rietveld refinement of XRD data we systematically studied the distribution of Pd ions as a function of calcination temperature between 550 and 900 °C. We also conducted DRIFTS experiments with CO as a probe molecule to interrogate the nature of Pd species present in this material after calcination in air at different temperatures.

The 1.8 wt% Pd/fer calcined at different temperatures was used in the H<sub>2</sub> TPR experiments in hydrated state without pretreatment to clearly distinguish the reduction of Pd ions at ~100 °C from the reduction of PdO clusters at 25-50 °C (Figure 2a).<sup>33, 57</sup> The Pd/fer-550C material has both PdO clusters and Pd ions in the form of Pd(OH)<sup>+</sup>, evidenced by the appearance of two reduction peaks at ~50 °C and at ~110 °C, respectively. The intensity of the low temperature reduction feature decreased dramatically after

air calcination at 700 °C and even further after 800 °C calcination and it completely disappeared after the 900 °C calcination. These changes are in agreement with the well-known dispersion of small PdO clusters inside the zeolite channels into charge compensating Pd ions upon high temperature calcination.<sup>39, 58-59</sup> This process is also confirmed by the IR data collected over these samples in the presence of CO (Figure 2b-c). The IR spectrum recorded from the 550 °C-calcined sample exhibited mostly a broad band centered at around 2140 cm<sup>-1</sup>, and has been assigned to CO adsorbed on Pd(OH)<sup>+</sup> ions in cationic positions.<sup>47</sup> This spectrum also shows a rather intense peak at ~1970 cm<sup>-1</sup> that represents CO molecules adsorbed in bridge-bonding configuration on metallic Pd particles. The intensity of the metallic Pd-bound CO signal is the highest for the Pd/FER sample calcined at the lowest (550 °C) temperature since this material has the largest amount of PdO present in its pores prior to CO exposure (CO readily reduces PdO clusters even at room temperature). There is a dramatic change in the IR spectrum collected from the sample calcined at 700 °C. Two doublet features develop at 2218 and 2200, as well as at 2215 and 2196 cm<sup>-1</sup>, while the intensity of the IR feature at ~2140 cm<sup>-1</sup> increased by a small extent. In contrast, the intensity of the IR band at ~1975 cm<sup>-1</sup> decreased extensively in this sample. These results indicate that upon calcination at 700 °C most of the PdO cluster present in the FER structure after lower temperature calcination re-disperse and form additional Pd(OH)<sup>+</sup> and new Pd<sup>2+</sup> ions located in cationic positions. This is also corroborated by the changes in the T-O-T vibrational region of the IR spectrum: the intensity of the IR band at 927 cm<sup>-1</sup> increased in the 700 °C-calcined sample, and then decreased when CO adsorbed onto Pd(OH)<sup>+</sup> sites (approximately by the same extent as in the 550 °C-calcined sample). Note that the position of this T-O-T vibrational feature is about 11 cm<sup>-1</sup> red shifted in comparison to that we have discussed above for the Pd/FER sample calcined at higher temperatures. The doublet features at high frequencies represent Pd<sup>2+</sup>(CO)<sub>2</sub> species, most probably occupying two different cationic positions or the same cationic position with altering Al distribution<sup>72</sup> in the FER structure. Calcination at even higher temperatures (800 and 900 °C) brings further changes in the IR spectra collected in the presence of CO flow. The most interesting change in the IR spectra is that in the T-O-T vibrational region: the feature that was observed at 927 cm<sup>-1</sup> blue shifts to 938 cm<sup>-1</sup> (as we have shown above in the discussion of the 900 °C-calcined material). What is even more interesting is that the intensity of this band changes only marginally after 800 °C calcination and not at all in 900 °C-calcined sample after exposure to CO. In the C-O vibrational region the intensity of the metallic Pd-bound CO signal (at 1975 cm<sup>-1</sup>) is absent when the sample is calcined at 900 °C, and the ionic Pd-bound CO bands decrease and almost disappears (both Pd<sup>2+</sup> and Pd(OH)<sup>+</sup>). The intensity of the T-O-T vibrational feature in the sample calcined at 900 °C is the highest indicating that the number of Pd ions interacting with the zeolite framework is the largest. By calcining the sample at 900 °C we maximized the number of Pd<sup>2+</sup> sites in the zeolite but minimized the amount of CO adsorbed. This controversial observation can be explained by the movement of Pd ions into cationic positions where they become coordinatively saturated that, in turn, prevents them from binding adsorbates (here CO and we have shown above NO as well). We also collected powder XRD patterns of the Pd/FER samples after *in situ* calcination at 550 and 800°C (Figure 2d) and observed no structural collapse of the zeolite framework. Difference Fourier maps were calculated (Figure 2e-f, Figure S2) from Rietveld refinements of these data against the unrefined FER framework.<sup>60</sup> For Pd/FER-550C, a cloud of electron density is distributed in both 10-membered ring channel and 6-membered ring, corresponding to the positions of PdO and Pd ions. In contrast, electron density is highly localized to the 6-membered ring after 800°C treatment where β-sites are located. The plot is consistent with our previous

interpretation that 1Al-bound Pd<sup>2+</sup>(OH) dispersed in both  $\alpha$ - and  $\beta$ -sites migrate to other cationic position in  $\beta$ -sites with 2Al by high temperature calcination. These results strongly suggest that the Pd ions unable to adsorb CO and NO from a dry gas stream after calcination above 800°C are located at 2Al sites in the 6-membered ring of the ferrierite cage.

## NO adsorption from dry and wet gas streams: the effect of calcination temperature

### a. NO adsorption in the absence of water

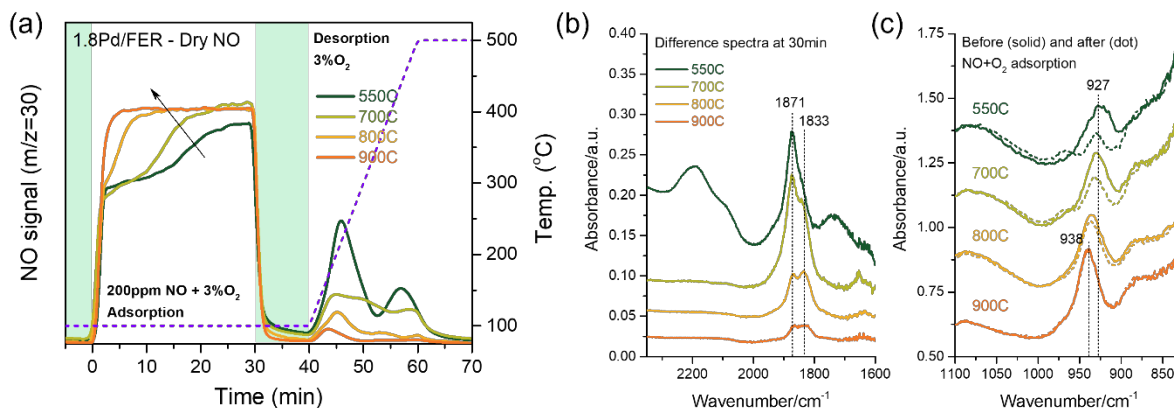


**Figure 3.** (a) NO adsorption and desorption curves for 1.8 wt.% Pd/FER calcined at various temperatures from 550 to 900°C measured by DRIFTS-MS. Adsorption gas contained 200 ppm NO+3% O<sub>2</sub> balance with He. (b) DRIFTS spectra after 30 min adsorption of dry NO. (c) Spectra obtained before and after dry NO adsorption for Pd/FER samples.

In the previous paragraphs we have shown how the temperature of calcination affected the nature of Pd species present in the FER zeolites and the effect of water on the NO adsorption properties of the Pd/FER sample calcined 900 °C. Here we present DRIFTS and MS results on the variation of NO adsorption properties of the 1.8 wt% Pd/FER material as a function of calcination temperature. Results obtained under both dry and wet NO uptake experiments are compared and contrasted.

A series of NO uptake/release profiles from a dry NO-containing gas stream on the 1.8 wt% Pd/FER sample calcined at 550, 700, 800 and 900 °C is displayed in Figure 3a. The uptake profiles (between 0 and 30 min) clearly show that the sample calcined at 550 °C has the highest NO uptake capacity. (The series of DRIFT spectra collected during the dry NO adsorption over this sample is shown in Figure S3.) The two main IR absorption features are located at 1871 and 2195 cm<sup>-1</sup>. The former band represents NO molecules adsorbed on Pd<sup>2+</sup>(OH) centers, while the latter one belongs to NO<sup>+</sup> ions that have replaced H<sup>+</sup> sites of the zeolite. With increasing calcination temperature the amount of NO adsorbed decreases gradually, and only a very small amount of NO is observed after calcination at 900 °C. The NO release profiles (40 to 70 min time interval in Figure 3a) are fully consistent with the uptake curves: under dry NO adsorption conditions the sample calcined at 550 °C releases the most NO, and the amount of NO<sub>x</sub> released gradually decreases with increasing sample calcination temperature. Beside the amount of NO<sub>x</sub> stored/released, the temperature where NO<sub>x</sub> is released also strongly influenced by the calcination temperature of the Pd/FER. Two distinct desorption features are observed for the 550 °C-calcined sample at ~200 and ~450 °C. The low temperature peak represents NO released mostly from NO<sup>+</sup>, while the high temperature one originates from NO

desorbing from ionic Pd sites. After 700 °C calcination the NO release profiles change dramatically. There is a very large drop in the amount of NO released at low temperature concomitant with sharp decline in the intensity of the IR band representing NO<sup>+</sup> (panel b of Figure 3). There is also a decrease in the intensity of the high temperature NO release feature and the development of a new band at an intermediate temperature (~300 °C), suggesting the formation of a new type of adsorption site. In the IR spectrum of the 700 °C-calcined material, beside the almost complete absence of the NO<sup>+</sup> feature, the shoulder on the lower frequency side of the main IR band becomes more prominent at 1833 cm<sup>-1</sup>. The amount of NO released from the 800 and 900 °C-calcined samples is very low in concert with the IR data that shows NO features with very low intensities. The results of our CO adsorption study discussed above can guide the assignment of the nitrosyl complexes formed in Pd/FER after NO exposure at 100 °C: after 550°C calcination mostly Pd<sup>2+</sup>(OH) (Figure 2b) species are present and form Pd<sup>2+</sup>(OH)-NO complexes. The main IR band at 1871 cm<sup>-1</sup> represents Pd<sup>2+</sup>(OH)-bound NO molecules in α-site while the small shoulder peak at 1833 cm<sup>-1</sup> can be assigned to Pd<sup>2+</sup>(OH)-bound NO molecules in β-site. This shoulder band at 1833 cm<sup>-1</sup> becomes more pronounced as the calcination temperature increases, while the intensities of the 1871 and 1833 cm<sup>-1</sup> features are comparable for the samples calcined 800 and 900 °C. The large decrease in the total integrated IR absorbance of these two latter peaks are consistent with the dramatically reduced NO uptake evidenced by the MS traces in Figure 3a. These results combined with the data discussed above for the CO adsorption, provide two important conclusions. First, Pd<sup>2+</sup>(OH) moieties are preferentially present near the α-site but high-temperature treatment makes them present at both α- and β-sites with similar probability. Second, during high temperature calcination Pd<sup>2+</sup>(OH) reacts with zeolitic OH groups and form Pd<sup>2+</sup> ions charge compensating 2AlO<sub>2</sub><sup>-</sup> sites. Due to the high coordination saturation of the thus formed Pd<sup>2+</sup> ions they become inaccessible for NO adsorption. Same trends are observed for the series of 0.5 wt.% Pd/FER calcined at different temperatures (Figure S4b-c).

Further evidence for the changes in the nature of ionic Pd species in the FER framework during high-temperature calcination is provided by changes in the shape and intensity of the asymmetric T-O-T vibrational feature of the zeolite framework. The variation of these peaks (both intensity and peak position) follows exactly the same trends we have discussed for CO adsorption. The broad band in the 1.8Pd/FER-550C sample is observed at 927 cm<sup>-1</sup>, which represents interaction between Pd<sup>2+</sup>(OH) and zeolite framework, and its intensity gradually decreases during dry NO adsorption. After calcination at 700°C the position of this IR feature remains almost unchanged, while its intensity increases, becomes sharper, and loses intensity upon NO adsorption. In the Pd/FER samples calcined at 800 and 900°C this T-O-T vibrational band is located at 938 cm<sup>-1</sup> with a blue shift of 11 cm<sup>-1</sup>. The shape of this band becomes much sharper possibly due to the interaction between the divalent Pd<sup>2+</sup> ion and 2AlO<sub>2</sub><sup>-</sup> sites in new cationic position. (The same phenomenon was observed in the low Pd loaded FER, compare results in Figure 3c and Figure S4c.) This shift in peak position is strong evidence that the interaction between Pd ions and the zeolite framework is altered during high temperature treatment. As the Pd ions move to thermodynamically more favorable cation positions during the high temperature calcination process the interaction between Pd ions and the zeolite framework becomes stronger. In the FER framework three different cationic positions have been proposed, i.e. α-, β-, and γ-sites, as illustrated in Figure S5.<sup>21, 61</sup> It has been established that the siting of various divalent cations, such as Fe<sup>2+</sup> or Co<sup>2+</sup>, on these three different cationic positions are reflected in the wavenumber of the perturbed T-O-T vibrational band.<sup>62-64</sup> The perturbed band with divalent

cations in  $\alpha$ -site has been observed at 935-950  $\text{cm}^{-1}$ , in  $\beta$ -site is 913-928  $\text{cm}^{-1}$ , and in  $\gamma$ -site at 879-905  $\text{cm}^{-1}$ .<sup>65</sup> Based on this, the newly formed divalent  $\text{Pd}^{2+}$  ions in FER after thermal treatment are highly likely to be located near  $\beta$ -site.

### b. NO adsorption in the presence of water and CO

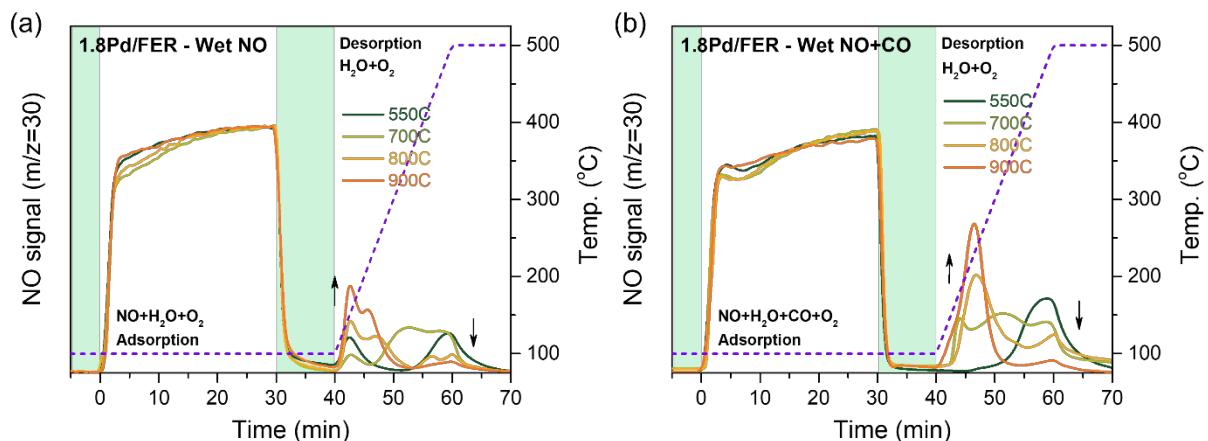


**Figure 4.** NO adsorption and desorption curves in the presence of (a)  $\text{H}_2\text{O}$  and both (b)  $\text{H}_2\text{O}$  and  $\text{CO}$  for 1.8 wt.% Pd/FER calcined at various temperatures from 550 to 900°C measured by DRIFTS-MS. Adsorption gas contained 200 ppm NO, 2.8%  $\text{H}_2\text{O}$ , 250ppm CO (when used), and 3%  $\text{O}_2$  balance with He.

The critical roles of water and CO in NO adsorption over the 900 °C-calcined Pd/FER sample have been discussed in the first part of this article (see Figure 1). The presence of water was necessary to achieve high NO uptake, and CO further enhanced the amount of NO adsorbed. The mechanism by which CO enhances NO adsorption has been studied extensively and clarified for Pd/CHA zeolites.<sup>48</sup> The effect of  $\text{H}_2\text{O}$  and CO on Pd/FER samples calcined at lower temperatures, however, have not been discussed yet. The NO uptake/release profiles for the Pd/FER materials calcined at 550, 700 and 900 °C in the presence  $\text{H}_2\text{O}$  and in the presence of both  $\text{H}_2\text{O}$  and CO are displayed in Figure 4. The NO uptake/release profile over the 1.8 wt.% Pd/FER-550C sample reveals a much smaller overall NO uptake capacity, and a dramatically reduced low temperature ( $\sim 200$  °C) NO release in comparison to those observed in the absence of  $\text{H}_2\text{O}$  (Figure 3). The very small amount of low temperature NO desorption is attributed to the hydration of Brønsted acid sites (i.e.,  $\text{H}^+$ ) in the zeolites that makes these sites unavailable for  $\text{NO}^+$  adsorption. The drop in the higher temperature NO release feature can be attributed to coordination of  $\text{H}_2\text{O}$  to the Pd ions in the zeolites and the reduced reactivity of these hydrated Pd ions with NO. As the Pd/FER material is calcined at increasingly higher temperature the shape of the NO release profiles changes significantly. In general, the intensity of the high temperature desorption peak decreases, while new low temperature desorption features develop. Interestingly, the total amount NO adsorbed did not vary systematically with the calcination temperature, it is similar for all four samples. The systematic shifts in the NO desorption temperature with the calcination temperature is the direct consequence of the ion redistribution among the cationic sites in the FER framework. The presence of both  $\text{H}_2\text{O}$  and CO in the gas mixture during NO adsorption enhances the overall NO uptake but does not significantly change the overall NO desorption profiles. The primary effect of CO is to enhance the amount of NO that can be adsorbed over these materials. As we have discussed above, Pd ions in the high temperature-calcined samples occupy cationic positions where they are strongly coordinated to the zeolite framework making them unreactive toward NO. The

desorption of NO takes place at about 400 °C from Pd/FER-550C, and it progressively moves to ~200 °C with increasing calcination temperature. Since Pd ions in the high temperature-calcined samples are strongly bound to the zeolite framework (and fully coordinated), they can only adsorb NO in their hydrated state when they interact with H<sub>2</sub>O that moves them out from their highly coordinated positions. The resulting hydrated nitrosyl complexes can easily decompose at 200 °C where Pd ions become dehydrated and move back to their highly coordinated positions. Such trend of temperature shift in NO desorption is observed in wet NO adsorption at low (0.5 wt.%) Pd loading (Figure S6) as well. The question about the nature of the Pd ions that are present in the FER zeolite after high temperature (>800 °C) calcination, however, still remains unanswered. Prior studies have proposed the presence of two different cationic  $\beta$ -sites in the FER structure.<sup>66-67</sup> Sklenak *et al.* found that Al pairs in T4 position, i.e.  $\beta$ -1 site, more strongly stabilize divalent cations than Al pairs in T2 position, i.e.  $\beta$ -2 site (Figure S5).<sup>66</sup> The consequence of this phenomenon is that cations located in the  $\beta$ -1 site interact weakly with guest molecules (i.e., adsorbates). It is known that the Al distributions on T4 and T2 positions vary greatly depending on the synthetic conditions of the FER zeolite.<sup>67-68,70</sup> We suggest that divalent Pd ions stabilized at the  $\beta$ -1 site are the ones that dominate in the Pd/FER-900C material and do not interact with NO in the absence of H<sub>2</sub>O in the gas stream. What is likely is that these divalent Pd ions are coordinated with four framework oxygen ions geometrically constrained within the 6-membered ring in a square planar geometry that is prevalent for metal complexes with  $d^8$  configuration.<sup>66,69</sup> Consequently, these Pd ions in constrained positions would not bind NO readily. However, in the presence of water Pd<sup>2+</sup> ions could shift due to insertion of water molecules between Pd and zeolite (hydration)<sup>44</sup> which would enable NO molecules to bind to these hydrated Pd ions. This is conceptually similar to what we have previously described for unusual cases when one of the adsorbates facilitates the adsorption of the second adsorbate.<sup>44,47,69</sup> This would clearly explain the necessity of water in NO adsorption over high temperature calcined Pd/FER storage materials. The large shift in the temperature of NO desorption over the high temperature-calcined Pd/FER samples is also consistent with the high stability of the adsorbate-free Pd ions in their square planar coordination: as water desorbs from the hydrated Pd ions they move back to their highly stable cationic positions while releasing NO at low (~200 °C) temperature. The phenomenon described in this work is expected to be useful for other metal/zeolite materials relevant to various adsorption applications.

## Conclusions

DRIFTS-MS and Rietveld refinement of XRD data were used to investigate the NO<sub>x</sub> adsorption ability of Pd ion-exchanged ferrierite-type zeolites after thermal treatments at various temperatures. The Pd ions located at the cationic positions of FER zeolite are present even after thermal treatment at 900 °C. Under dry stream containing NO and oxygen, Pd ions become unable to bind NO as the calcination temperature increases above 700 °C. In contrast, Pd ions readily adsorb NO under wet stream containing NO, H<sub>2</sub>O, and oxygen and are converted into hydrated Pd-NO complexes. The addition of CO to the wet stream further promotes the amount of NO adsorption on Pd ions. We found that this unusual behavior arises from high temperature-induced relocation of Pd<sup>2+</sup>(OH) into divalent Pd ions in more stable cationic position, probably  $\beta$ -1 site, in 6-membered ring of ferrierite cage. Such phenomenon is evidenced by the change in perturbed skeletal (T-O-T) vibration band, probe molecule (CO and NO) adsorptions, and Rietveld refinement results of *in situ* XRD data. Hydrated nitrosyl complexes of relocated Pd ions

[Pd(NO)(H<sub>2</sub>O)<sub>x</sub> and/or Pd(NO)(CO)(H<sub>2</sub>O)<sub>x</sub>] in new cationic positions can readily release NO at about 200 °C where dehydration of the Pd-aqua complex occurs, which is in the operating temperature range of deNO<sub>x</sub> catalysts.

### **Acknowledgments**

The authors gratefully acknowledge the US Department of Energy (DOE), Energy Efficiency and Renewable Energy, Vehicle Technologies Office for the support of this work. The research described in this paper was performed in the Environmental Molecular Sciences Laboratory (EMSL), a national scientific user facility sponsored by the DOE's Office of Biological and Environmental Research and located at Pacific Northwest National Laboratory (PNNL). PNNL is operated for the US DOE by Battelle.

## References

1. Corma, A. State of the art and future challenges of zeolites as catalysts. *J. Catal.* **2003**, 216 (1-2), 298-312.
2. Davis, M. E.; Lobo, R. F. Zeolite and molecular sieve synthesis. *Chem. Mater.* **1992**, 4 (4), 756-768.
3. Newsam, J. The zeolite cage structure. *Science* **1986**, 231 (4742), 1093-1099.
4. Von Ballmoos, R.; Meier, W. Zoned aluminium distribution in synthetic zeolite ZSM-5. *Nature* **1981**, 289 (5800), 782-783.
5. Dai, H.; Shen, Y.; Yang, T.; Lee, C.; Fu, D.; Agarwal, A.; Le, T. T.; Tsapatsis, M.; Palmer, J. C.; Weckhuysen, B. M. Finned zeolite catalysts. *Nat. Mater.* **2020**, 19 (10), 1074-1080.
6. Perea, D. E.; Arslan, I.; Liu, J.; Ristanović, Z.; Kovarik, L.; Arey, B. W.; Lercher, J. A.; Bare, S. R.; Weckhuysen, B. M. Determining the location and nearest neighbours of aluminium in zeolites with atom probe tomography. *Nat. Commun.* **2015**, 6 (1), 1-8.
7. Pitman, M. C.; Van Duin, A. C. Dynamics of confined reactive water in smectite clay-zeolite composites. *J. Am. Chem. Soc.* **2012**, 134 (6), 3042-3053.
8. Fasano, M.; Humplik, T.; Bevilacqua, A.; Tsapatsis, M.; Chiavazzo, E.; Wang, E. N.; Asinari, P. Interplay between hydrophilicity and surface barriers on water transport in zeolite membranes. *Nat. Commun.* **2016**, 7 (1), 1-8.
9. Lee, Y.; Vogt, T.; Hriljac, J. A.; Parise, J. B.; Hanson, J. C.; Kim, S. J. Non-framework cation migration and irreversible pressure-induced hydration in a zeolite. *Nature* **2002**, 420 (6915), 485-489.
10. Zhang, J.; Wang, L.; Zhang, B.; Zhao, H.; Kolb, U.; Zhu, Y.; Liu, L.; Han, Y.; Wang, G.; Wang, C. Sinter-resistant metal nanoparticle catalysts achieved by immobilization within zeolite crystals via seed-directed growth. *Nat. Catal.* **2018**, 1 (7), 540-546.
11. Ravi, M.; Sushkevich, V. L.; van Bokhoven, J. A. Towards a better understanding of Lewis acidic aluminium in zeolites. *Nat. Mater.* **2020**, 19 (10), 1047-1056.
12. Corma, A.; Diaz-Cabanas, M. J.; Martínez-Triguero, J.; Rey, F.; Rius, J. A large-cavity zeolite with wide pore windows and potential as an oil refining catalyst. *Nature* **2002**, 418 (6897), 514-517.
13. Khivantsev, K.; Jaegers, N.; Kovarik, L.; Kwak, J.-H.; Derewinski, M.; Szanyi, J. On the nature of extra-framework aluminum species and improved catalytic properties in steamed zeolites. *Molecules* **2022**, 27, 2352. <https://doi.org/10.3390/molecules27072352>. Song, I.; Lee, H.; Jeon, S. W.; Ibrahim, I. A.; Kim, J.; Byun, Y.; Koh, D. J.; Han, J. W.; Kim, D. H. Simple physical mixing of zeolite prevents sulfur deactivation of vanadia catalysts for NO<sub>x</sub> removal. *Nat. Commun.* **2021**, 12 (1), 1-9.
15. Pfriem, N.; Hintermeier, P. H.; Eckstein, S.; Kim, S.; Liu, Q.; Shi, H.; Milakovic, L.; Liu, Y.; Haller, G. L.; Baráth, E. Role of the ionic environment in enhancing the activity of reacting molecules in zeolite pores. *Science* **2021**, 372 (6545), 952-957.
16. Khivantsev, K.; Jaegers, N. R.; Aleksandrov, H. A.; Kovarik, L.; Derewinski, M. A.; Wang, Y.; Vayssilov, G. N.; Szanyi, J. Biomimetic CO oxidation below- 100° C by a nitrate-containing metal-free microporous system. *Nat. Commun.* **2021**, 12 (1), 1-8.
17. Bregante, D. T.; Chan, M. C.; Tan, J. Z.; Ayla, E. Z.; Nicholas, C. P.; Shukla, D.; Flaherty, D. W. The shape of water in zeolites and its impact on epoxidation catalysis. *Nat. Catal.* **2021**, 4 (9), 797-808.
18. Cronstedt, A. Natural zeolite and minerals. *Svenska Vetenskaps Akademiens Handlingar Stockholm* **1756**, 17, 120.
19. Hack, J. H.; Dombrowski, J. P.; Ma, X.; Chen, Y.; Lewis, N. H.; Carpenter, W. B.; Li, C.; Voth, G. A.; Kung, H. H.; Tokmakoff, A. Structural Characterization of Protonated Water Clusters Confined in HZSM-5 Zeolites. *J. Am. Chem. Soc.* **2021**, 143 (27), 10203-10213.
20. Hattori, H.; Shiba, T. The nature of the acid sites on cationized zeolites: characterization by infrared study of adsorbed pyridine and water. *J. Catal.* **1968**, 12 (2), 111-120.

21. Dalconi, M. C.; Alberti, A.; Cruciani, G. Cation migration and structural modification of Co-exchanged ferrierite upon heating: a time-resolved X-ray powder diffraction study. *J. Phys. Chem. B* **2003**, 107 (47), 12973-12980.
22. Louisfremea, W.; Paillaud, J.-L.; Porcher, F.; Perrin, E.; Onfroy, T.; Massiani, P.; Boutin, A.; Rotenberg, B. Cation migration and structural deformations upon dehydration of nickel-exchanged NaY zeolite: A combined neutron diffraction and Monte Carlo study. *J. Phys. Chem. C* **2016**, 120 (32), 18115-18125.
23. Zema, M.; Tarantino, S.; Montagna, G. Hydration/dehydration and cation migration processes at high temperature in zeolite chabazite. *Chem. Mater.* **2008**, 20 (18), 5876-5887.
24. Khivantsev, K.; Jaegers, N. R.; Aleksandrov, H. A.; Kovarik, L.; Song, I.; Tian, J.; Hernandez, X. I. P.; Vayssilov, G. N.; Wang, Y.; Szanyi, J. Identification of single Ru (II) ions on ceria as a highly active catalyst for abatement of NO<sub>x</sub> pollutants. *Chemrxiv* **2021**, 10.33774/chemrxiv-2021-vr21g-v2.
25. Petrov, A. W.; Ferri, D.; Krumeich, F.; Nachttegaal, M.; van Bokhoven, J. A.; Kröcher, O. Stable complete methane oxidation over palladium based zeolite catalysts. *Nat. Commun.* **2018**, 9 (1), 1-8.
26. Paolucci, C.; Khurana, I.; Parekh, A. A.; Li, S.; Shih, A. J.; Li, H.; Di Iorio, J. R.; Albarracin-Caballero, J. D.; Yezerets, A.; Miller, J. T. Dynamic multinuclear sites formed by mobilized copper ions in NO<sub>x</sub> selective catalytic reduction. *Science* **2017**, 357 (6354), 898-903.
27. Lee, H.; Song, I.; Jeon, S. W.; Kim, D. H. Mobility of Cu Ions in Cu-SSZ-13 Determines the Reactivity of Selective Catalytic Reduction of NO<sub>x</sub> with NH<sub>3</sub>. *J. Phys. Chem. Lett.* **2021**, 12 (12), 3210-3216.
28. Lee, H.; Song, I.; Jeon, S. W.; Kim, D. H. Inter-particle migration of Cu ions in physically mixed Cu-SSZ-13 and H-SSZ-13 treated by hydrothermal aging. *React. Chem. Eng.* **2019**, 4 (6), 1059-1066.
29. Gao, F.; Mei, D.; Wang, Y.; Szanyi, J.; Peden, C. H. Selective catalytic reduction over Cu/SSZ-13: linking homo-and heterogeneous catalysis. *J. Am. Chem. Soc.* **2017**, 139 (13), 4935-4942.
30. Millan, R.; Cnudde, P.; Van Speybroeck, V.; Boronat, M. Mobility and Reactivity of Cu<sup>+</sup> Species in Cu-CHA Catalysts under NH<sub>3</sub>-SCR-NO<sub>x</sub> Reaction Conditions: Insights from AIMD Simulations. *JACS Au* **2021**, 1 (10), 1778-1787.
31. Zheng, Y.; Kovarik, L.; Engelhard, M. H.; Wang, Y.; Wang, Y.; Gao, F.; Szanyi, J. n. Low-temperature Pd/zeolite passive NO<sub>x</sub> Adsorbers: structure, performance, and adsorption chemistry. *J. Phys. Chem. C* **2017**, 121 (29), 15793-15803.
32. Khivantsev, K.; Gao, F.; Kovarik, L.; Wang, Y.; Szanyi, J. n. Molecular Level Understanding of How Oxygen and Carbon Monoxide Improve NO<sub>x</sub> Storage in Palladium/SSZ-13 Passive NO<sub>x</sub> Adsorbers: The Role of NO<sup>+</sup> and Pd (II)(CO)(NO) Species. *J. Phys. Chem. C* **2018**, 122 (20), 10820-10827.
33. Lee, J.; Kim, J.; Kim, Y.; Hwang, S.; Lee, H.; Kim, C. H.; Kim, D. H. Improving NO<sub>x</sub> storage and CO oxidation abilities of Pd/SSZ-13 by increasing its hydrophobicity. *Appl. Catal. B: Environ.* **2020**, 277, 119190.
34. Lee, J.; Kim, Y.; Hwang, S.; Lee, E.; Lee, H.; Kim, C. H.; Kim, D. H. Deactivation of Pd/Zeolites passive NO<sub>x</sub> adsorber induced by NO and H<sub>2</sub>O: Comparative study of Pd/ZSM-5 and Pd/SSZ-13. *Catal. Today* **2021**, 360, 350-355.
35. Villamaina, R.; Iacobone, U.; Nova, I.; Tronconi, E.; Ruggeri, M. P.; Mantarosie, L.; Collier, J.; Thompsett, D. Mechanistic insight in NO trapping on Pd/Chabazite systems for the low-temperature NO<sub>x</sub> removal from Diesel exhausts. *Appl. Catal. B: Environ.* **2021**, 284, 119724.
36. Gu, Y.; Majumdar, S. S.; Pihl, J. A.; Epling, W. S. Investigation of NO adsorption and desorption phenomena on a Pd/ZSM-5 passive NO<sub>x</sub> adsorber. *Appl. Catal. B: Environ.* **2021**, 298, 120561.
37. Kunal, P.; Toops, T. J.; Kidder, M. K.; Lance, M. J. Deactivation trends of Pd/SSZ-13 under the simultaneous presence of NO, CO, hydrocarbons and water for passive NO<sub>x</sub> adsorption. *Appl. Catal. B: Environ.* **2021**, 299, 120591.
38. Chen, H.-Y.; Collier, J. E.; Liu, D.; Mantarosie, L.; Durán-Martín, D.; Novák, V.; Rajaram, R. R.; Thompsett, D. Low temperature NO storage of zeolite supported Pd for low temperature diesel engine emission control. *Catal. Lett.* **2016**, 146 (9), 1706-1711.

39. Ryou, Y.; Lee, J.; Cho, S. J.; Lee, H.; Kim, C. H.; Kim, D. H. Activation of Pd/SSZ-13 catalyst by hydrothermal aging treatment in passive NO adsorption performance at low temperature for cold start application. *Appl. Catal. B: Environ.* **2017**, *212*, 140-149.
40. Khivantsev, K.; Jaegers, N. R.; Kovarik, L.; Hanson, J. C.; Tao, F.; Tang, Y.; Zhang, X.; Koleva, I. Z.; Aleksandrov, H. A.; Vayssilov, G. N. Achieving Atomic Dispersion of Highly Loaded Transition Metals in Small-Pore Zeolite SSZ-13: High-Capacity and High-Efficiency Low-Temperature CO and Passive NO<sub>x</sub> Adsorbers. *Angew. Chem. Int. Ed.* **2018**, *57* (51), 16672-16677.
41. Khivantsev, K.; Jaegers, N. R.; Kovarik, L.; Proding, S.; Derewinski, M. A.; Wang, Y.; Gao, F.; Szanyi, J. Palladium/Beta zeolite passive NO<sub>x</sub> adsorbers (PNA): Clarification of PNA chemistry and the effects of CO and zeolite crystallite size on PNA performance. *Appl. Catal. A: Gen.* **2019**, *569*, 141-148.
42. Khivantsev, K.; Jaegers, N. R.; Kovarik, L.; Hu, J. Z.; Gao, F.; Wang, Y.; Szanyi, J. Palladium/zeolite low temperature passive NO<sub>x</sub> adsorbers (PNA): structure-adsorption property relationships for hydrothermally aged PNA materials. *Emission Contr. Sci. Technol.* **2020**, *6* (2), 126-138.
43. Mandal, K.; Gu, Y.; Westendorff, K. S.; Li, S.; Pihl, J. A.; Grabow, L. C.; Epling, W. S.; Paolucci, C. Condition-dependent Pd speciation and NO adsorption in Pd/zeolites. *ACS Catal.* **2020**, *10* (21), 12801-12818.
44. Khivantsev, K.; Jaegers, N. R.; Koleva, I. Z.; Aleksandrov, H. A.; Kovarik, L.; Engelhard, M.; Gao, F.; Wang, Y.; Vayssilov, G. N.; Szanyi, J. Stabilization of super electrophilic Pd<sup>2+</sup> cations in small-pore SSZ-13 zeolite. *J. Phys. Chem. C* **2019**, *124* (1), 309-321.
45. Khivantsev, K.; Jaegers, N. R.; Kovarik, L.; Wang, M.; Hu, J. Z.; Wang, Y.; Derewinski, M. A.; Szanyi, J. The superior hydrothermal stability of Pd/SSZ-39 in low temperature passive NO<sub>x</sub> adsorption (PNA) and methane combustion. *Appl. Catal. B: Environ.* **2021**, *280*, 119449.
46. Kim, Y.; Sung, J.; Kang, S.; Lee, J.; Kang, M.-H.; Hwang, S.; Park, H.; Kim, J.; Kim, Y.; Lee, E. Uniform synthesis of palladium species confined in a small-pore zeolite via full ion-exchange investigated by cryogenic electron microscopy. *J. Mater. Chem. A* **2021**.
47. Khivantsev, K.; Wei, X.; Kovarik, L.; Jaegers, N. R.; Walter, E. D.; Tran, P.; Wang, Y.; Szanyi, J. Pd/FER vs Pd/SSZ-13 Passive NO<sub>x</sub> Adsorbers: Adsorbate-controlled Location of Atomically Dispersed Pd(II) in FER Determines High Activity and Stability. *Angew. Chem. Int. Ed.* **2022**, *134* (3), e202107554.
48. Song, I.; Khivantsev, K.; Wang, Y.; Szanyi, J. Elucidating the Role of CO in the NO Storage Mechanism on Pd/SSZ-13 with in Situ DRIFTS. *J. Phys. Chem. C* **2021**.
49. Ozensoy, E.; Goodman, D. W. Vibrational spectroscopic studies on CO adsorption, NO adsorption CO+ NO reaction on Pd model catalysts. *Phys. Chem. Chem. Phys.* **2004**, *6* (14), 3765-3778.
50. Chakarova, K.; Ivanova, E.; Hadjiivanov, K.; Klissurski, D.; Knözinger, H. Co-ordination chemistry of palladium cations in Pd-H-ZSM-5 as revealed by FTIR spectra of adsorbed and co-adsorbed probe molecules (CO and NO). *Phys. Chem. Chem. Phys.* **2004**, *6* (013), 3702-3709.
51. Castoldi, L.; Matarrese, R.; Morandi, S.; Ticali, P.; Lietti, L. Low-temperature Pd/FER NO<sub>x</sub> adsorbers: operando FT-IR spectroscopy and performance analysis. *Catal. Today* **2021**, *360*, 317-325.
52. Kwak, J. H.; Varga, T.; Peden, C. H.; Gao, F.; Hanson, J. C.; Szanyi, J. Following the movement of Cu ions in a SSZ-13 zeolite during dehydration, reduction and adsorption: A combined in situ TP-XRD, XANES/DRIFTS study. *J. Catal.* **2014**, *314*, 83-93.
53. Broclawik, E.; Datka, J.; Gil, B.; Kozyra, P. T-O-T skeletal vibration in CuZSM-5 zeolite: IR study and quantum chemical modeling. *Phys. Chem. Chem. Phys.* **2000**, *2* (3), 401-405.
54. Sobalik, Z.; Šponer, J. E.; Wichterlová, B. In *Studies in Surface Science and Catalysis*, Elsevier: 2000; Vol. 130, pp 1463-1468.
55. Sárkány, J.; Sachtler, W. M. In *Studies in Surface Science and Catalysis*, Elsevier: 1995; Vol. 94, pp 649-656.
56. Millan, R.; Cnudde, P.; Hoffman, A. E.; Lopes, C. W.; Concepción, P.; Van Speybroeck, V.; Boronat, M. Theoretical and Spectroscopic Evidence of the Dynamic Nature of Copper Active Sites in Cu-CHA

- Catalysts under Selective Catalytic Reduction (NH<sub>3</sub>-SCR-NO<sub>x</sub>) Conditions. *J. Phys. Chem. Lett.* **2020**, *11* (23), 10060-10066.
57. Lardinois, T. M.; Bates, J. S.; Lippie, H. H.; Russell, C. K.; Miller, J. T.; Meyer III, H. M.; Unocic, K. A.; Prikhodko, V.; Wei, X.; Lambert, C. K. Structural Interconversion between Agglomerated Palladium Domains and Mononuclear Pd (II) Cations in Chabazite Zeolites. *Chem. Mater.* **2021**, *33* (5), 1698-1713.
58. Okumura, K.; Niwa, M. Regulation of the dispersion of PdO through the interaction with acid sites of zeolite studied by extended X-ray absorption fine structure. *J. Phys. Chem. B* **2000**, *104* (41), 9670-9675.
59. Homeyer, S.; Sachtler, W. Oxidative redispersion of palladium and formation of PdO particles in NaY: An Application of High Precision TPR. *Appl. Catal.* **1989**, *54* (1), 189-202.
60. Morris, R. E.; Weigel, S. J.; Henson, N. J.; Bull, L. M.; Janicke, M. T.; Chmelka, B. F.; Cheetham, A. K. A synchrotron X-ray diffraction, neutron diffraction, <sup>29</sup>Si MAS-NMR, and computational study of the siliceous form of zeolite ferrierite. *J. Am. Chem. Soc.* **1994**, *116* (26), 11849-11855.
61. Ivanova, E.; Mihaylov, M.; Hadjiivanov, K.; Blasin-Aubé, V.; Marie, O.; Plesniar, A.; Daturi, M. Evidencing three distinct FeII sites in Fe-FER zeolites by using CO and NO as complementary IR probes. *Appl. Catal. B: Environ.* **2010**, *93* (3-4), 325-338.
62. Sobalík, Z.; Dědeček, J.; Ikonnikov, I.; Wichterlová, B. State and coordination of metal ions in high silica zeolites Incorporation, development and rearrangement during preparation and catalysis. *Microporous Mesoporous Mater.* **1998**, *21* (4-6), 525-532.
63. Sobalík, Z.; Tvarůžková, Z.; Wichterlová, B. Skeletal T-O-T vibrations as a tool for characterization of divalent cation complexation in ferrierite. *J. Phys. Chem. B* **1998**, *102* (7), 1077-1085.
64. Sobalík, Z.; Dědeček, J.; Kaucký, D.; Wichterlová, B.; Drozdová, L.; Prins, R. Structure, Distribution, and Properties of Co Ions in Ferrierite Revealed by FTIR, UV-Vis, and EXAFS. *J. Catal.* **2000**, *194* (2), 330-342.
65. Olszowka, J. E.; Lemishka, M.; Mlekodaj, K.; Kubat, P.; Rutkowska-Zbik, D.; Dedecek, J.; Tabor, E. Determination of Zn Speciation, Siting, and Distribution in Ferrierite Using Luminescence and FTIR Spectroscopy. *J. Phys. Chem. C* **2021**, *125* (17), 9060-9073.
66. Sklenak, S.; Andrikopoulos, P. C.; Whittleton, S. R.; Jirglova, H.; Sazama, P.; Bencko, L.; Bucko, T.; Hafner, J.; Sobalik, Z. Effect of the Al siting on the structure of Co (II) and Cu (II) cationic sites in ferrierite. A periodic DFT molecular dynamics and FTIR study. *J. Phys. Chem. C* **2013**, *117* (8), 3958-3968.
67. Dedecek, J.; Lucero, M. J.; Li, C.; Gao, F.; Klein, P.; Urbanova, M.; Tvaruzkova, Z.; Sazama, P.; Sklenak, S. Complex analysis of the aluminum siting in the framework of silicon-rich zeolites. A case study on ferrierites. *J. Phys. Chem. C* **2011**, *115* (22), 11056-11064.
68. Pinar, A. B.; Rzepka, P.; Knorpp, A. J.; McCusker, L. B.; Baerlocher, C.; Huthwelker, T.; van Bokhoven, J. A. Pinpointing and Quantifying the Aluminum Distribution in Zeolite Catalysts Using Anomalous Scattering at the Al Absorption Edge. *J. Am. Chem. Soc.* **2021**.
69. Jaegers, N. R.; Khivantsev, K.; Kovarik, L.; Klas, D. W.; Hu, J. Z.; Wang, Y.; Szanyi, J. *Catal. Sci. Technol.* **2019**, *9* (23), 6570-6576.
70. Khivantsev, K.; Derewinski, M. A.; Jaegers, N. R.; Boglajenko, D.; Hernandez, X. I. P.; Pearce, C.; Wang, Y.; Szanyi, J. *Chemrxiv* **2021**, 10.26434/chemrxiv.14038388.v1

Supplementary Information for

## Unusual water-assisted NO adsorption over Pd/FER calcined at high temperatures: The effect of cation migration

Inhak Song,<sup>a</sup> Konstantin Khivantsev,<sup>a\*</sup> Yiqing Wu,<sup>a</sup> Mark Bowden,<sup>a</sup> Yong Wang,<sup>a,b</sup> and János Szanyi<sup>a\*</sup>

<sup>a</sup>Institute for Integrated Catalysis, Pacific Northwest National Laboratory, Richland, Washington 99352, United States

<sup>b</sup>Voiland School of Chemical Engineering and Bioengineering, Washington State University, Pullman, Washington 99164, United States

\*Corresponding author: konstantin.khivantsev@pnnl.gov and janos.szanyi@pnnl.gov

### Materials and Methods

#### List of supplementary figures

**Figure S1.** (a) DRIFTS spectra of H/FER zeolites calcined at 550, 800, and 900°C. The spectra were collected at 100°C after dehydration at 500°C under 3% O<sub>2</sub>/He.

**Figure S2.** Difference electron density map in y-direction plotted from Rietveld refinement for Pd/FER pre-treated at 550 and 800°C. X-ray diffraction patterns of Pd/FER were obtained at 200°C after in situ thermal oxidative treatments at 550 and 800°C.

**Figure S3.** (a) DRIFTS spectra obtained during dry NO adsorption at 100°C for 30 min. Before experiment, the sample was dehydrated at 500°C for 30 min under 3% O<sub>2</sub>/He. Adsorption gas contains 200 ppm NO + 3% O<sub>2</sub>. (b) DRIFTS spectra obtained during wet NO+CO adsorption at 100°C for 30 min. Adsorption gas contains 200 ppm NO, 250 ppm CO, 2.8% H<sub>2</sub>O, and 3% O<sub>2</sub>.

**Figure S4.** (a) NO adsorption and desorption curves for 0.5 wt.% Pd/FER calcined at various temperatures from 550 to 900°C measured by DRIFTS-MS. Adsorption gas contained 200 ppm NO+3% O<sub>2</sub> balance with He. (b) DRIFTS spectra after 30 min adsorption of dry NO. (c) Spectra obtained before and after dry NO adsorption for Pd/FER samples.

**Figure S5.** Ferrierite-type framework structure. The positions of the geometrically four different tetrahedral sites (T1 to T4) are shown. Three different cationic sites have been proposed, denoted as  $\alpha$ -,  $\beta$ -, and  $\gamma$ -type sites. The  $\alpha$  site is coordinated to the 10-ring channels, while  $\beta$  site is located at the center of the six-membered ring. The  $\gamma$  site is located inside the ferrierite cage.

**Figure S6.** Wet NO adsorption and desorption curves for 0.5 wt.% Pd/FER calcined at various temperatures from 550 to 900°C measured by DRIFTS-MS. Adsorption gas contained 200 ppm NO, 3% O<sub>2</sub>, and 2.8% H<sub>2</sub>O balance with He. Desorption of adsorbed NO<sub>x</sub> was performed under wet stream (3% O<sub>2</sub>+2.8% H<sub>2</sub>O/He) with the ramping rate of 20°C/min.

## Materials and Methods

Pd/FER zeolite powder with 1.8 wt.% Pd loading was made by incipient wetness impregnation method. Commercial NH<sub>4</sub>-form FER-type zeolite with Si:Al~10 was supplied by Zeolyst, and 10 wt.% tetraamine palladium(II) nitrate solution in H<sub>2</sub>O was used for preparation. Normally, about 1 g of NH<sub>4</sub>-FER powder was dried in an oven at 70°C for 1 h before impregnation. Targeted amount of palladium precursor solution was slowly added, i.e. 10 μL at once by using pipet, to NH<sub>4</sub>-FER powder with continuous mixing and mild grinding. The resulting powder was dried in an oven at 70°C overnight, and subsequently calcined in air at 550°C for 5 h with the ramp-up rate of 2°C/min, which is designated as 1.8Pd/FER-550C. This yellowish powder was calcined again at 700, 800, and 900°C for 5 h with the ramp-up rate of 10°C/min. The color of yellowish powder becomes brighter as calcination temperature increases. The prepared Pd/FER samples are stored in ambient conditions.

The *in situ* diffuse reflectance IR measurements were performed in a commercial DRIFTS cell with ZnSe window. The spectra were collected on Nicolet iS50 FT-IR (Thermo Fisher Scientific Co., USA) spectrometer equipped with a liquid nitrogen-cooled MCT detector. Each spectrum was obtained as the average of 32 scans with 4 cm<sup>-1</sup> resolution. A background spectrum was recorded with KBr powder at temperatures where measurements were conducted. The space through which the IR beam passes on both sides of the reactor window was continuously purged with nitrogen to maintain a constant background. The sample cup inside DRIFTS cell was filled with α-alumina powder in a typical experiment. After that, a thin layer of Pd/FER powder was spread over it and pressed firmly. Gas stream through the DRIFTS cell was controlled by mass flow controllers. Moisture was added by flowing the gas through a glass bubbler filled with distilled water. In each and every experiment, 0.025 g of powder was loaded, and the flow rate was adjusted to 100 mL/min (GHSV~240,000 mL·g<sup>-1</sup>·h<sup>-1</sup>). The outlet of the DRIFTS cell was connected to a quadrupole mass spectrometer (Hiden Analytical).

H<sub>2</sub>-temperature programmed reduction (H<sub>2</sub>-TPR) of the Pd/FER materials were performed on a AutoChem II 2920 chemisorption analyzer equipped with an TCD detector. The measurements were conducted on hydrated samples without pretreatment. Typically, the experiments were conducted from -70 to 400°C at 10°C/min in 10% H<sub>2</sub>/Ar (OXARC, Inc., UHP).

Powder XRD patterns were collected using a Panalytical MRD Bragg-Brentano goniometer fitted with an Anton Parr HTK-1200 high temperature stage. Cu Kα radiation was used, along with variable divergence and anti-scatter slits, and a post-diffraction monochromator. Patterns were collected at 0.04° intervals between 5 and 100°2θ, scanning at 0.25 °2θ/min. The sample was heated to 550 °C and cooled to 25 °C under flowing O<sub>2</sub> before collection. A second heating under O<sub>2</sub> to 800 °C and return to 25 °C was carried out before the second acquisition. Collecting the data near room temperature reduced the influence of thermal vibrations as well as stage offsets arising from thermal expansion. Rietveld refinement was carried out using Topas v6 (Bruker AXS) and the ferrierite structure published by Cheetham *et al.* (Morris, R. E.; Weigel, S. J.; Henson, N. J.; Bull, L. M.; Janicke, M. T.; Chmelka, B. F.; Cheetham, A. K. A synchrotron X-ray diffraction, neutron diffraction, <sup>29</sup>Si MAS-NMR, and computational study of the siliceous form of zeolite ferrierite. *J. Am. Chem. Soc.* **1994**, 116 (26), 11849-11855.)

Only the scale factor and lattice parameters of ferrierite were refined, and difference Fourier maps output for visualization using VESTA. (Momma, K.; Izumi, F. VESTA 3 for three-dimensional visualization of crystal, volumetric and morphology data. *Journal of applied crystallography* **2011**, 44 (6), 1272-1276.)

The positive electron density difference isosurfaces were plotted for  $0.4 \text{ e}/\text{\AA}^3$ .

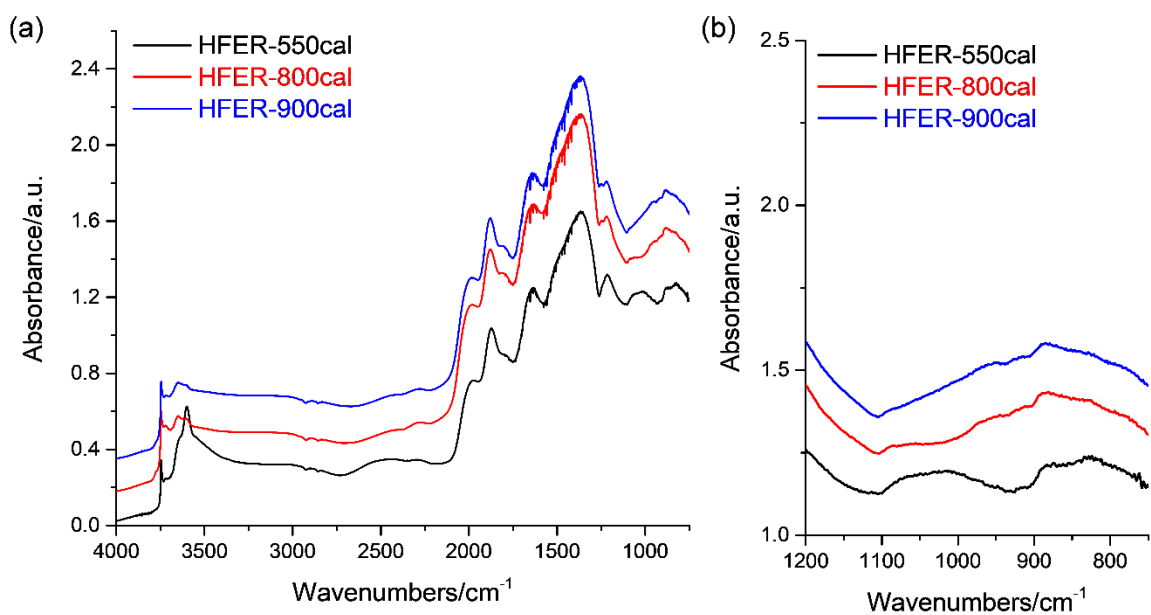


**Figure S1.** (a) DRIFTS spectra of H/FER zeolites calcined at 550, 800, and 900°C. The spectra were collected at 100°C after dehydration at 500°C under 3%  $\text{O}_2/\text{He}$ .

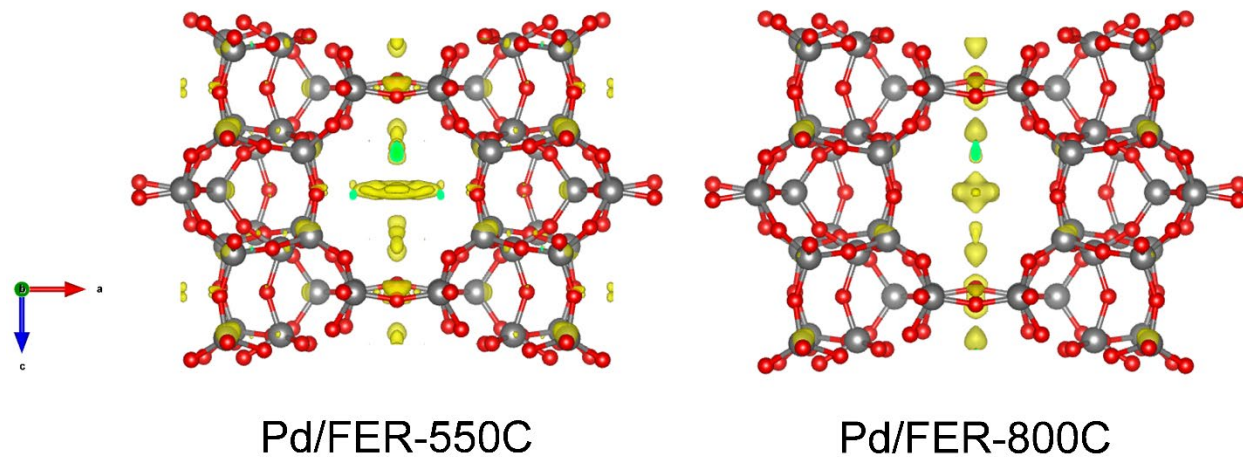


**Figure S2.** Difference electron density map viewed along [010] plotted from Rietveld refinement for Pd/FER pre-treated at 550 and 800 °C. X-ray diffraction patterns of Pd/FER were obtained at 25 °C after in situ thermal oxidative treatments at 550 and 800 °C.

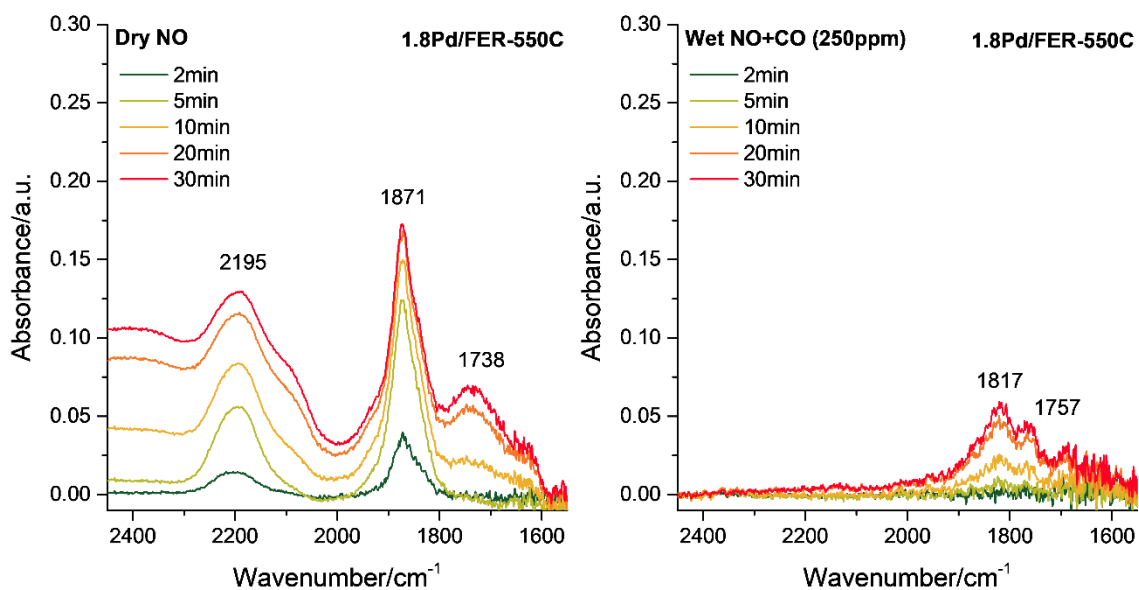


**Figure S3.** (a) DRIFTS spectra obtained during dry NO adsorption at 100°C for 30 min. Before experiment, the sample was dehydrated at 500°C for 30 min under 3% O<sub>2</sub>/He. Adsorption gas contains 200 ppm NO + 3% O<sub>2</sub>. (b) DRIFTS spectra obtained during wet NO+CO adsorption at 100°C for 30 min. Adsorption gas contains 200 ppm NO, 250 ppm CO, 2.8% H<sub>2</sub>O, and 3% O<sub>2</sub>.

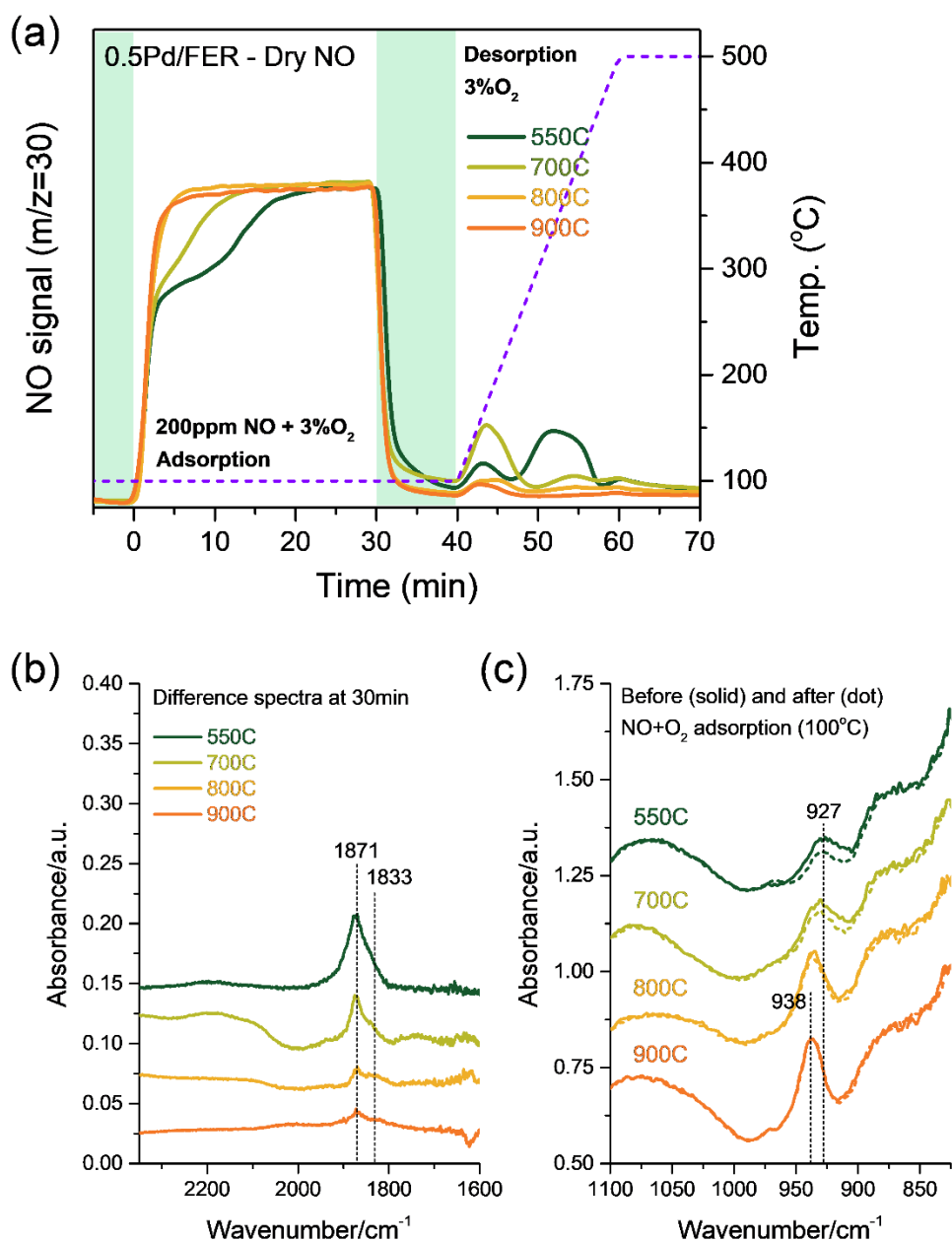


**Figure S4.** (a) NO adsorption and desorption curves for 0.5 wt.% Pd/FER calcined at various temperatures from 550 to 900  $^{\circ}\text{C}$  measured by DRIFTS-MS. Adsorption gas contained 200 ppm NO+3%  $\text{O}_2$  balance with He. (b) DRIFTS spectra after 30 min adsorption of dry NO. (c) Spectra obtained before and after dry NO adsorption for Pd/FER samples.

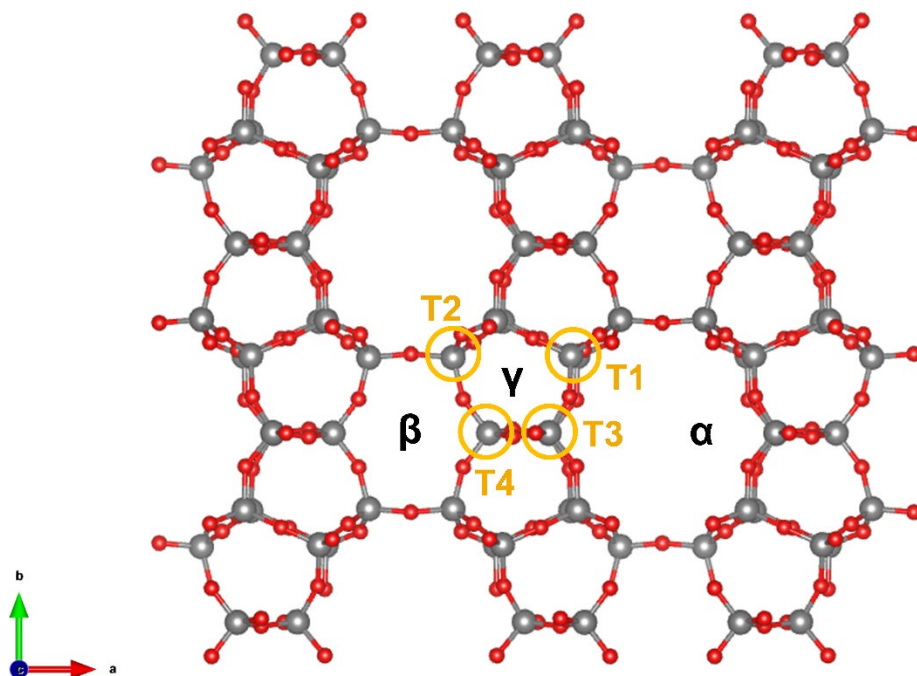


**Figure S5.** Ferrierite-type framework structure. The positions of the geometrically four different tetrahedral sites (T1 to T4) are shown. Three different cationic sites have been proposed, denoted as  $\alpha$ -,  $\beta$ -, and  $\gamma$ -type sites. The  $\alpha$  site is coordinated to the 10-ring channels, while  $\beta$  site is located at the center of the six-membered ring. The  $\gamma$  site is located inside the ferrierite cage.

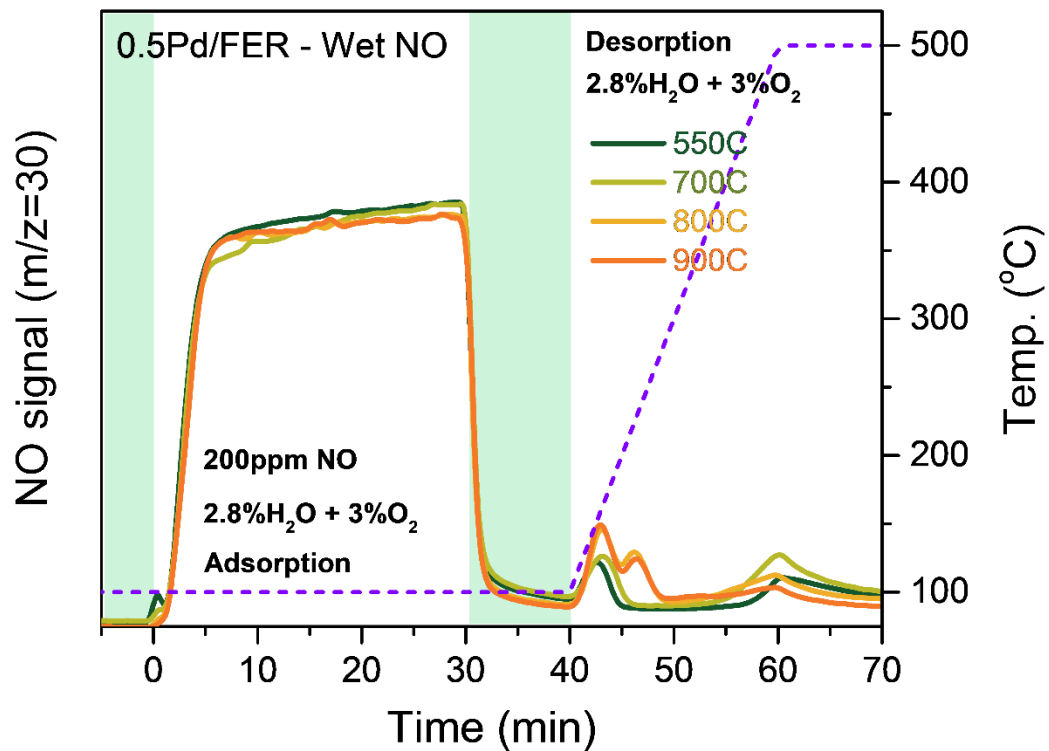


**Figure S6.** Wet NO adsorption and desorption curves for 0.5 wt.% Pd/FER calcined at various temperatures from 550 to 900°C measured by DRIFTS-MS. Adsorption gas contained 200 ppm NO, 3% O<sub>2</sub>, and 2.8% H<sub>2</sub>O balance with He. Desorption of adsorbed NO<sub>x</sub> was performed under wet stream (3% O<sub>2</sub>+2.8% H<sub>2</sub>O/He) with the ramping rate of 20°C/min.